International Journal of Thin Films Science and Technology

http://dx.doi.org/10.18576/ijtfst/150202

A Comprehensive Study on Damage Behavior of ZnO-TiO_2 Coatings on Photovoltaic Panels Under Simulated Desert Wind Conditions

Ali Ooda Abd[1,2,], Anas Bouguecha[1] and Mohamed Haddar[1]*

[1] Laboratory of Mechanics Modeling and Production, National Engineering School of Sfax, University of Sfax, Sfax, Tunisia
[2] Department of Applied Physics, College of Applied Sciences, University of Technology, Baghdad, Iraq

Received: 22 Feb. 2026, Revised: 12 Apr. 2026, Accepted: 26 Apr. 2026
Published online: 1 May 2026

Abstract: This study evaluates the mechanical durability and solid particle erosion (SPE) behavior of a 50%-50% ZnO-TiO_2 nanocomposite coating designed for protective, self-cleaning solar applications. Nanoparticles synthesized via hydrolysis were deposited onto glass substrates using thermal spraying to a 1 µm thickness. The coating's structural, morphological, and chemical properties were rigorously characterized using (XRD)**,** (SEM)**,** (EDX)**,** and (AFM)**.** Erosion resistance was tested at impact angles of 15°, 30°, 45°, and 60°. The composite material exhibited a high maximum transmittance of 94% in the visible and infrared (VIS-IR) spectral range. The erosion rate increased with the impact angle, rising from ~0.0004 mg/g at 15° to ~0.0016 mg/g at 60°**.** The erosion mechanism is governed by brittle fracture mechanics, where higher impact angles promote crack propagation and material spallation. These results serve as a vital reference for enhancing the longevity of solar modules in sand-intensive environments.

Keywords: ZnO-TiO_2 nanocomposite. Solid particle erosion. impact angle.

1. Introduction

The global transition toward renewable energy has established solar photovoltaics (PV) as a critical technology for reducing greenhouse gas emissions [1-3]. However, the operational efficiency of PV panels is severely hindered by environmental factors, most notably "soiling," where the accumulation of atmospheric dust on the module surface can reduce power output by up to 50% in arid and desert regions [4-7]. Beyond simple light obstruction, windblown sand causes significant mechanical erosion, resulting in surface scratches and cracks that permanently degrade the optical transmittance and structural integrity of the encapsulating glass [1-9]. To mitigate these losses, researchers have developed various anti-soiling and self-cleaning coatings, with metal oxides such as (TiO_2) and (ZnO) emerging as leading candidates due to their excellent photocatalytic properties, mechanical stability, and high visible-light transparency [10-13]. Research indicates that solid-particle erosion behavior is highly dependent on the impingement angle; while brittle materials like coating materials typically exhibit maximum mass loss at a normal impact angle (90°), ductile materials peak at acute angles (15°–30°), and reinforced composites often show a semi-ductile response peaking between 45° and 60° [14-17]. Despite these advancements, a significant gap remains in the current literature regarding the specific damage behavior and durability of 50%-50% ZnO-TiO_2 composite coatings. While the individual properties of these oxides are well-documented, there is a lack of detailed analysis on how their hybrid formulation responds to varying impact angles under desert-like erosive conditions. Understanding the relationship between erosion and impact angle for this specific composite is essential to ensure the long-term durability of protective coatings in harsh environments [18-20].

1.2. State of the art.

ZnO-TiO_2 nanocomposites represent a state-of-the-art class of multifunctional thin films increasingly deployed for photo catalytic degradation, self-cleaning surfaces, and the enhancement of optical transmittance in photovoltaic (PV) modules [1-4]. Current literature trends indicate that modulating the crystalline structure specifically the phase transition between amorphous, anatase, and rutile TiO_2 significantly impacts functional efficiency by altering bandgap energies and reducing electron-hole recombination rates [5-7]. To evaluate the mechanical integrity of these metal-oxide films, solid particle erosion (SPE) testing is traditionally utilized, often following ASTM G76 standards to map mass loss or volumetric wear as a function of particle velocity and impingement angle [8-10]. These methodologies traditionally distinguish between ductile mechanisms (peaking at 15°–30°) and brittle fracture mechanics (peaking at 90°) to estimate the lifespan of protective ceramic coatings [11-13]. Critical Challenges and Gaps Despite functional advancements, several critical bottlenecks persist in the current domain Structural

*Corresponding author E-mail: hamedalwan14@gmail.com

Vulnerability and Brittleness: The inherent brittleness of the $ZnO-TiO_2$ matrix makes it susceptible to aggressive micro abrasive wear. Under high-velocity impact, material erosion is primarily driven by the intersection of lateral and radial cracks, leading to rapid surface degradation [14-16]. Delamination Tendencies High-angle impingement often induces severe delamination and "tunnel erosion," where vertical stress components cause the film to shed irregularly from the glass substrate, compromising its protective utility [17,18]. Stoichiometric Performance Gaps There is a notable deficiency in empirical data regarding the mechanical durability of the specific 50%-50% $ZnO-TiO_2$ hybrid, as most research focuses on pure components or low-concentration dopants [19,20]. Testing this specific composite on a controlled erosion testing apparatus directly bridges the gap between purely chemical / photocatalytic evaluations and real-world mechanical durability, ensuring functional longevity in harsh, sand-intensive environments [21]. This study article simulates in full the features of the oxide erosion of materials by sand. The damage process of sand erosion was also explored in detail. The study might be an essential reference for the improvement of power generating efficiency and maintenance schedule of photovoltaic power plants.

2. Materials and experimental Study.

2.1. Practical Part

Nanoparticles of both Zinc oxide and titanium oxide were prepared by hydrolysis at a molar concentration of 0.1 M .(0.81 and 2.33) grams respectively of each material were dissolved in 100 mL of non-ionic water using a hot stirrer at 70°C for two hours. After obtaining the nanoparticle solution, it was deposited onto glass slides (2.5 x 2.5) cm as shown in Fig (1) by thermal spraying to a thickness of approximately 1 µm. The thickness was measured gravimetrically. The samples were tested for deposited on glass using zinc oxide with titanium oxide to determine the hardness range.

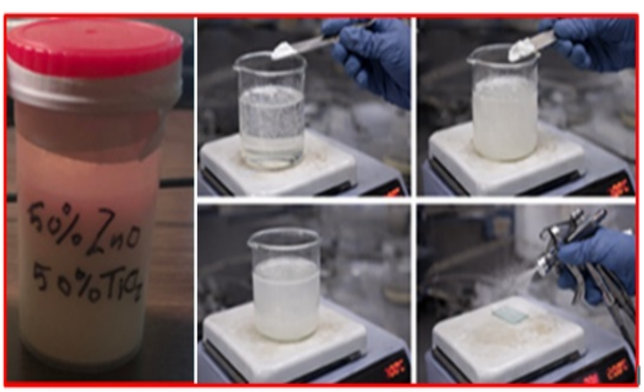

Fig. 1: Nanoparticles ZnO 50%-TiO_2 50% prepared by hydrolysis.

2.2. Erosion Experiments and Impact Studies.

2.2.1. Methods and Apparatus of the Experiment

The experimental platform created in this part is a desert wind and sand erosion simulation system. The structure of the experimental platform is depicted in Fig (2) [14].

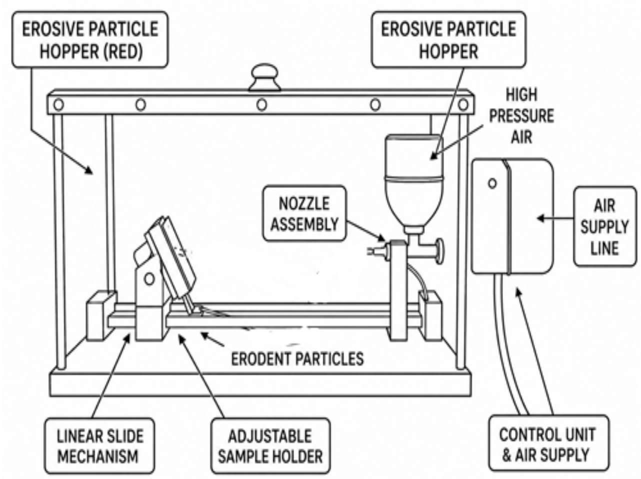

Fig. 2: Simulation system of desert wind and sand erosion.

As seen in Fig (2), the experimental platform is made up of an air compressor, airflow control valves, a sandbox, a sandblasting gun, an erosion chamber, and a recycling container. The experimental process is as follows: first, air compressors are used to provide a hight-pressure airflow, and airflow control valves are used to control the erosion rate produced by this flow; second, the sandblasting gun is used to direct the sandflow from the sandbox and mix it with the hight-pressure airflow into the erosion chamber; finally, the abraded sand particles are collected in the recycling container and recycled for use in other experiments. The comparison of the glass sample sprayed with 50%-50% $ZnO-TiO_2$ before and after erosion requires the accurate measurement of the mass of the sample before and after the experiment using a precision electronic balance. This section presents the analysis at the erosion velocity of sand and dust of 4 m/s. The selected abrasion angles are 15°, 30°, 45° and 60° to study the effect of sand and dust erosion on photovoltaic module and its performance parameters. The erosion experiment was limited to 30 min because of the small size of the sand particles (90um) used and the long time required for the erosion process of the coating film by wind and sand [14].

2.2.2. Evaluation of Erosion Results

The degree of erosion damage to the PV module can be characterized by the relative erosion rate E_0 [20], which is expressed as shown in (1).

$$E_0 = m_1 - m_2 / m_1 \quad (1)$$

Where: m_1 : mas of sample before erosion

m_2 : mas of sample after erosion

3. Results and Discussion

The XRD pattern of the TiO_2-ZnO nano-composite is depicted in the provided Fig (3). The diffraction peaks provide direct evidence that the substance that was synthesized is of a crystalline type. In the vicinity of 25.3 degrees, the strong diffraction peak corresponds to the (101) plane of anatase TiO_2; on the other hand, the peaks that are placed at around 31.7 degrees, 34.4 degrees, 36.2 degrees, 47.5 degrees, 56.6 degrees, 62.8 degrees, and 67.9 degrees are indexed to the hexagonal wurtzite structure of zinc oxide. The nanocomposite exhibits a high phase purity, as evidenced by the absence of major impurity peaks. Following the use of Scherrer's equation, it was determined that the average crystallite size was somewhere between 31 and 33 nanometers. Interference construction monochromatic rays reflected from any point of lattice levels at specific angles make up X-ray diffraction peaks. The distance interfaces between the diffraction angle levels at a particular peak can be found by using Bragg's law [22].

$$n\,\lambda = 2d\,\sin\theta_B \tag{2}$$

where n is an integer representing the degree of interference (n=1,2,3), The X-ray's wavelength is 1.54Å, the Bragg's angle is θ, and the distance between diffracting surfaces is d. Typically, XRD is used to compute several parameters that could be utilized to shed light on the deposited film research. Since it is equal to the width of the line profile (in radians) at half of the greatest intensity, the FWHM of the preferred orientation (peak) might be measured [23]. The single line approach is one of several line profile analysis procedures based on a Voigt function to determine the size–strain parameters (micro-strains and crystallite sizes). The average crystallite size (D) can be estimated using Scherrer's formula [24].

$$D = \frac{0.94\,\lambda}{\beta\,cos(\theta)} \tag{3}$$

The c-lattice constant of the structure deviates from the ASTM value due to microstrains that are created during the formation of thin films and are raised by stretching or compression in the lattice. Therefore, different atom displacements with respect to their reference lattice position are what generate the strain broadening (102). The formula (4) can be used to compute this strain:

$$\eta = \frac{C_{ASTM} - C_{XRD}}{C_{ASTM}} \;X\; 100\,\% \tag{4}$$

Where: C_{ASTM} Lattice constant by standard ASTM card and C_{XRD} Lattice constant measurement by XRD.

(η) can be calculated using the following relation (5):

$$\delta \;= \frac{1}{D^2} \quad (\text{lines/nm})^2 \tag{5}$$

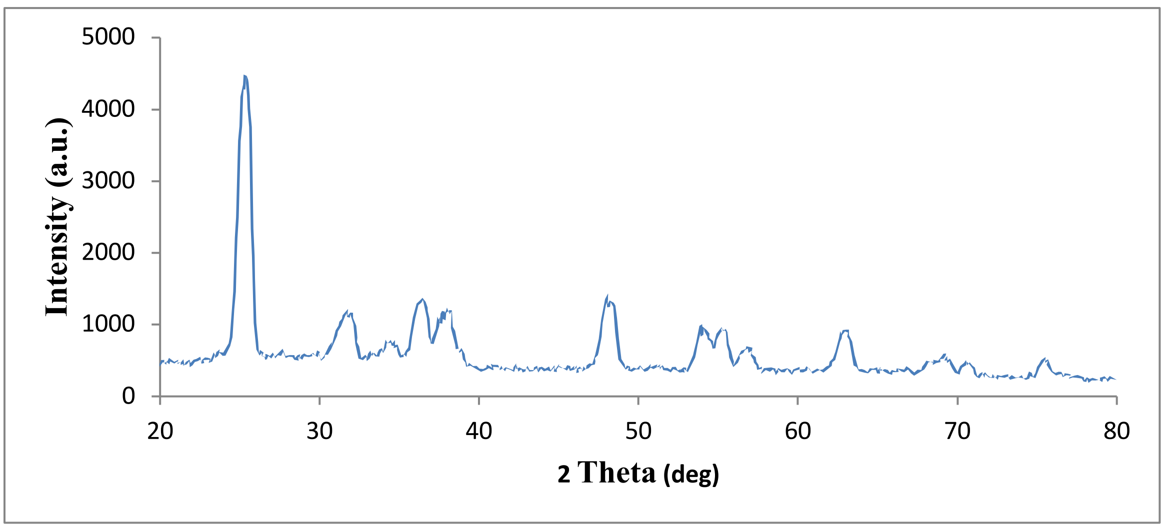

Fig. 3: XRD pattern of the TiO_2 50%-ZnO 50% nanocomposite

Table 1: Structural parameters obtained from XRD analysis of TiO_2-ZnO nanocomposite.

2θ (deg)	**(hkl) Plane**	**Phase**	**d observed (Å)**	**d standard (Å)**	**FWHM (deg)**	**D (nm)**	**δ ×10⁻⁴ (lines·m⁻²)**	**η ×10⁻⁴ (lines²·m⁻⁴)**
25.32	(101)	TiO_2 (Anatase)	3.51	3.52	0.27	31.21	10.26	11.59
31.77	(100)	ZnO	2.81	2.81	0.25	33.25	9.04	10.88
34.42	(002)	ZnO	2.6	2.6	0.28	31.08	10.34	11.64
36.25	(101)	ZnO	2.48	2.47	0.29	30.02	11.1	12.15
47.54	(200)	TiO_2 (Anatase)	1.91	1.89	0.31	28.07	12.69	13.42
56.6	(110)	ZnO	1.62	1.63	0.3	29	11.89	12.88
62.86	(204)/(103)	TiO_2/ZnO	1.48	1.48	0.33	26.42	14.33	14.91

Fig (4) indicates the recorded absorption spectra of ZnO 50%-TiO_2 50% colloidal solutions function of wavelength. It observed that the absorption is highest in the UV- region (short wavelengths corresponding to high photon energy) and sharply declines as wavelength increases. This phenomenon is explained by the interaction of light photons with the material, which promotes electrons from the valence band to the conduction band by absorbing photons with energy equal to or greater than the optical band gap. Lower absorption values occur from a decrease in the likelihood of electronic transitions when photon energy falls at longer wavelengths. ZnO-TiO_2 has a high transmittance in the VIS-IR spectrum; at wavelengths between 400 and 1100 nm, ZnO-TiO_2 had the maximum transmittance of 94%, indicating its potential for usage in solar systems.

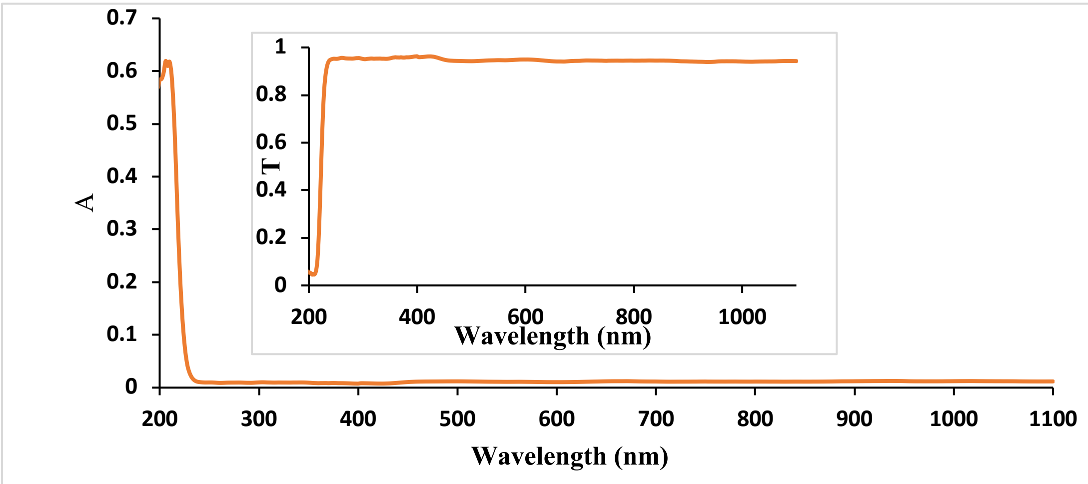

Fig. 4: Absorption and Transmittance spectra of ZnO 50%-TiO_2 50% nanocomposite

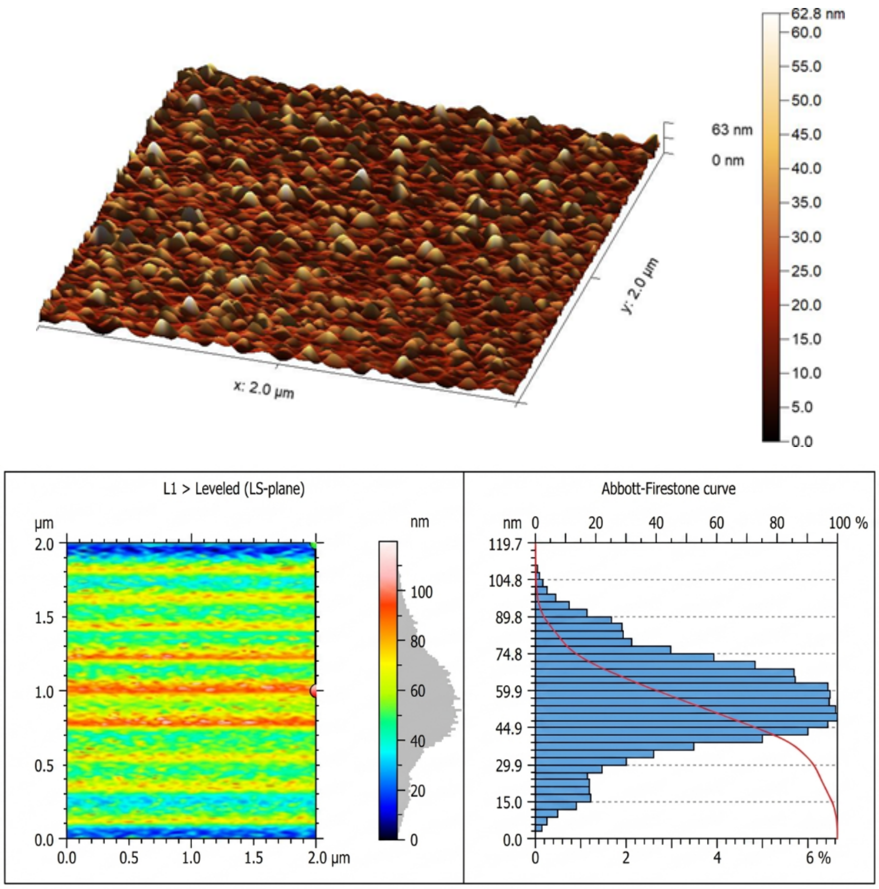

Fig. 5: 3D AMF Images and chart distribution for ZnO-TiO2 nanocomposite before erosion

AFM micrographs were taken utilizing digital instruments, Inc. Nanoscope and Dimension 3100 to evaluate the surface roughness and topography of deposited thin films. AFM imaging data are root mean square (RMS) roughness and grain size. It has three major forms of topography mapping: touch, non-contact (used in our morphology investigation) and intermittent contact or tapping. The tip with its nanometer radius of curvature is the most critical part of an AFM. The tip is linked to a microscale cantilever that responds to the van der Waals force and other forces between the tip and the sample. The $ZnO\text{-}TiO_2$ film before and after erosion analysis using atomic force microscopy (AFM) with special software (Imager 4.62). Fig (5) shows 3D FM image the surface topography data analyzed using powerful atomic microscopy (AFM) or a similar optical/pencil topography technique. This section presents three-dimensional surface maps along with elevation distribution histograms and Abbott-Firestone curves. These micro- or nano-maps show the surface of $ZnO\text{-}TiO_2$ over a defined area (2μm × 2μm). The color bars indicate surface roughness elevation characteristics ranging from 0 to approximately 20 nm (top image) and up to 60 nm (bottom image). Abbott-Firestone curves and histograms (right panels): Blue histograms: Show the statistical distribution of surface data points at different elevation levels. Red S-curves (Abbott-Firestone curve): Represent the cumulative probability distribution of the surface profile elevations. This program describes the material content as a function of depth, which is very useful for analyzing surface, loading zone characteristics, and fluid retention capacity. The main metrics and standards typically extracted from this program, several basic functional surface roughness parameters are calculated: (Sq= 58nm) and the average grin size = 59.9 nm).

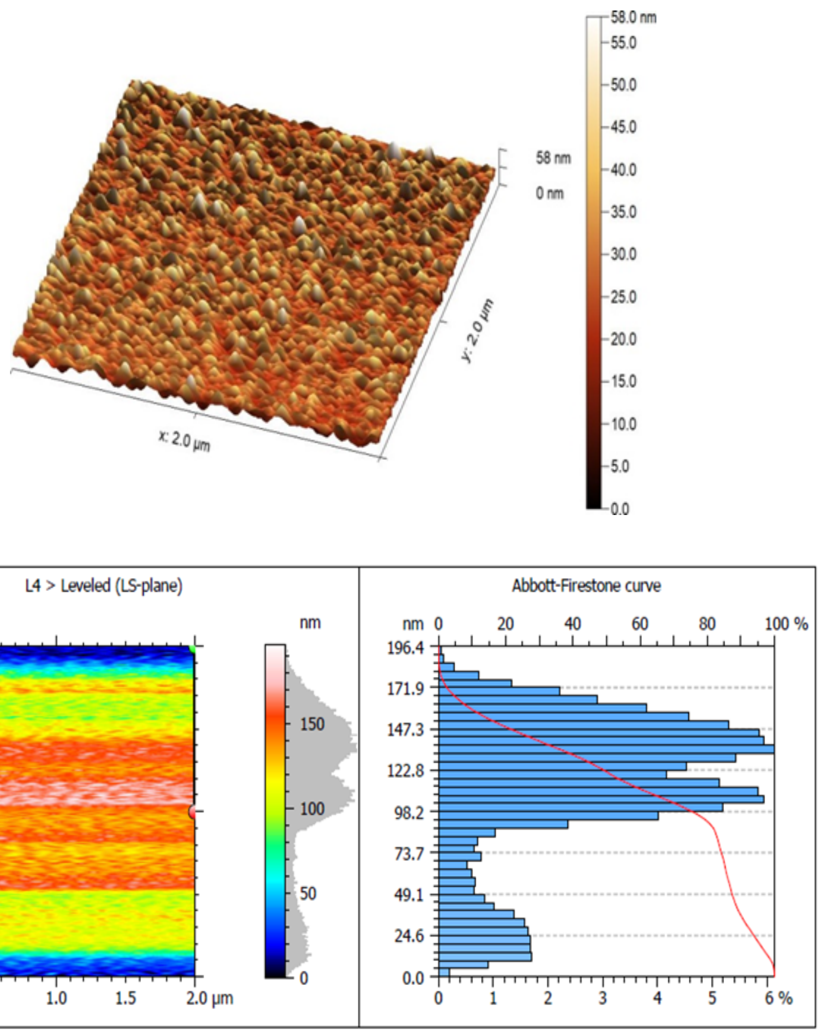

Fig. 6: 3D AMF Images and chart distribution for $ZnO\text{-}TiO_2$ nanocomposite after erosion

Fig (6) shows zinc oxide and titanium films after erosion. It is observed that the film was not completely removed from any location in the deposited layer, consistent with the SEM results, with a slight increase in roughness and a decrease in average particle size to ... nanometers.

(Fig 7,a) shows the morphological characteristics of dissolved Zinc oxide (ZnO) and titanium dioxide (TiO_2) nanoparticles at a concentration of (0.1) M which is deposited on glass substrate (25 x 25) mm^2 has different particles sizes. Clear differences in particle size can be observed from the images.

The diameter of booth the Zinc oxide (ZnO) and titanium dioxide (TiO_2) nanoparticles is (50-200) nm.

It consists of nanoparticles with various geometric shapes, such as spherical or silica-like forms. Visual features indicate the presence of closely packed, small grains, consistent with scanning electron microscopy (SEM) images of nanomaterials. This is particularly true for (ZnO) and (TiO_2) particles. The homogeneity and regularity of the film deposited on the glass indicate a suitable preparation and deposition method, resulting in surfaces with strong hardness and cohesion. There is no evidence of dislocations, cracks, or interstitial spaces, and the deposition temperature does not generate any defects in the film.

(ZnO) and (TiO_2) both possess exceptional properties, including high photo-catalytic activity, stability, and antimicrobial efficacy, making them preferred semiconductors for the analysis of organic pollutants in water bodies. However, their large band gap and rapid electron-gap recombination limit their photo-catalytic activity. Consequently, decorating the surface of ZnO and TiO_2 with metallic nanoparticles such as r (Ag), (Pt), (Pd), and (Au) has garnered significant attention to overcome these limitations These metallic nanoparticles have gained considerable interest due to their characteristic localized surface plasmon resonance (LSPR) effect, which allows for enhanced absorption of visible light, and their ability to trap electrons, which facilitates efficient charge separation by slowing down electron-gap recombination and thus increasing photo catalytic activity. At the interface between semiconductors (such as zinc oxide and titanium dioxide) and metal nanoparticles, a Schottky surface forms due to work function differences and energy band alignment, typically leading to the separation and transport of photoexcited charge carriers. Thus, the incorporation of semiconductors with metal nanoparticles alters the electron-gap charge carrier pathways and their recombination rate, thereby improving the overall photo catalytic efficiency [25,26].

(Fig 7,b) shows (SEM) images of ZnO-TiO_2 Nano composites typically reveal a heterogeneous structure combining ZnO rods or nanoparticles with TiO_2 Nano spheres. These images highlight the surface distribution, agglomeration, and specific nanostructures of the materials. Explore these official, peer-reviewed resources for typical SEM images, structural analyses, and morphological properties.

Sandblasting (abrasive blasting) is used in industry as a destructive method to assess the adhesion strength of films and coatings to surfaces, to test mechanical durability. The goal of this procedure is to cause damage to the coating in order to gauge its strength. A high-pressure stream of sand or other abrasive material is directed at the film as part of the test mechanism. The objective is to measure the force or pressure required to remove or peel the coating from the surface, reflecting the quality of the preparation. As shown in the figure, after sandblasting the ZnO-TiO_2 film, a large surface area composed of nanoparticles is removed, and the remaining particles are fragmented into spherical or semi-spherical particles with dimensions not exceeding 70 nanometers, as illustrated in the Fig (b) . In the case of the composite ZnO-TiO_2, we observe that the effects of blasting and particle fragmentation were present, but the strong adhesive force prevented the erosion of the lower layers of the membrane. Compared to the previous figure, we note that no gaps or complete localized removal will appear, as shown in the Fig (b).

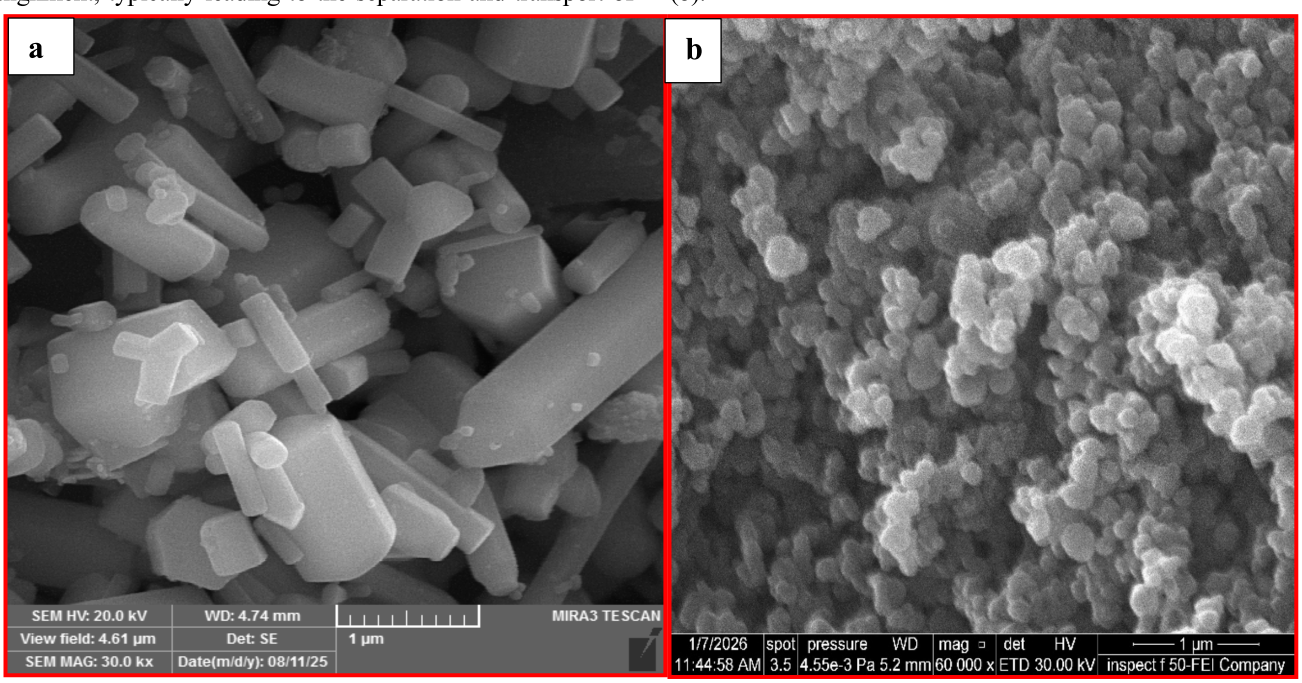

Fig. 7: a: Image of ZnO-TiO_2 nanocomposite before erosion, b: Image of ZnO-TiO_2 nanocomposite after erosion.

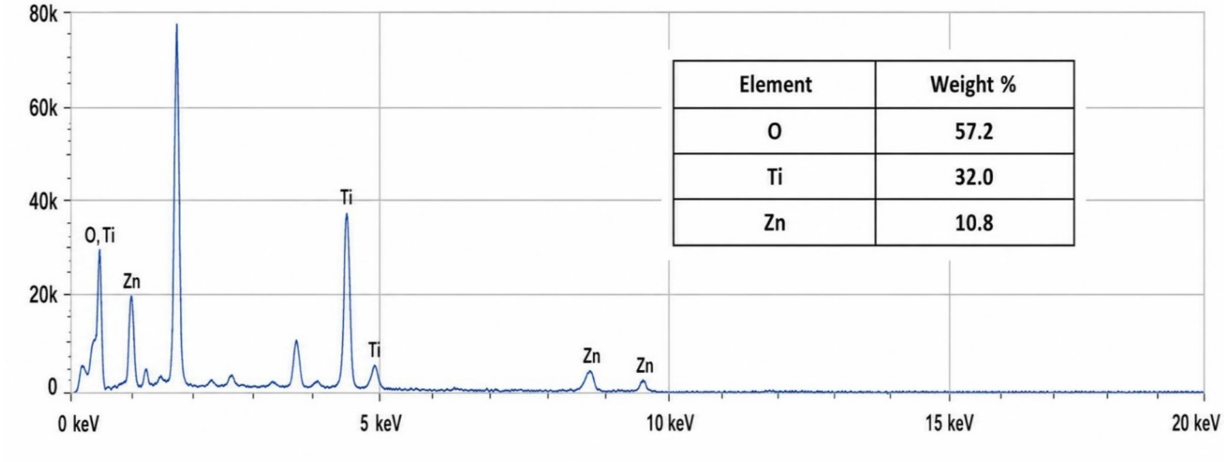

Element	Weight %
O	57.2
Ti	32.0
Zn	10.8

Fig. 8: EDX Spectra of ZnO-TiO2 nanocomposite before erosion.

Fig (8) (EDS or EDX) spectrum, which is used to determine the elemental composition of a sample. The main features of the spectrum are: the x-axis (horizontal), representing the energy of the X-rays measured in kilo electron volts (keV); the y-axis (vertical), representing the intensity or counting rate of the detected X-rays; and the peaks, each sharp peak indicating a specific element present in the sample. (EDX) for ZnO-TiO_2 (Zinc Oxide-Titanium Dioxide) composites confirms elemental composition and purity. It identifies the presence of Zinc (Zn), Titanium (Ti), and Oxygen (O), and maps their spatial distribution without additional impurities. Characteristic Peaks In an EDX spectrum, you will typically see distinct X-ray emission peaks corresponding to specific energy levels: Titanium (Ti): Kα ≈ 4.51 keV, Kβ ≈ 4.93 keV , Zinc (Zn): Lα ≈ 1.01 keV, Kα ≈ 8.63 keV, Kβ ≈ 9.57 keVOxygen (O): Kα ≈ 0.52 keV.

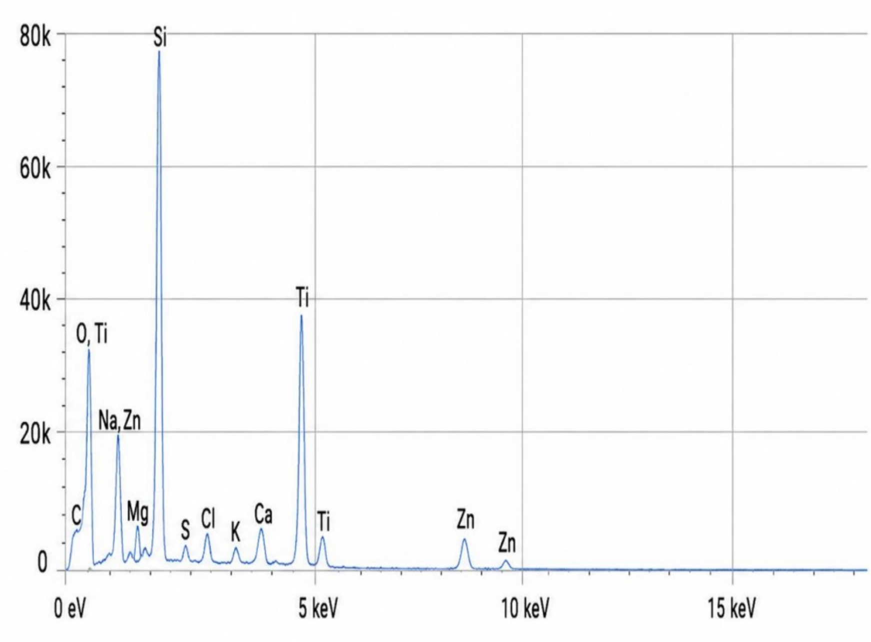

Element	Weight %
C	12.8
O	37.2
Na	3.2
Mg	1.4
Si	18.9
S	0.5
Cl	0.7
K	0.4
Ca	3.2
Ti	16.6
Zn	5.2

Fig. 9: EDX Spectra of ZnO-TiO2 nanocomposite after erosion.

Fig (9). shows the results of EDS analysis of sample ZnO-TiO_2, showing the X-ray energy on the x-axis and the signal intensity on the y-axis. The table inset lists the elements detected in the sample and their weight percentages, with carbon (C) at 12.6%, oxygen (O) at 37.2%, silicon (Si) at 18.9%, and titanium (Ti) at 16.6% being the main elements. The peaks of the graph clearly indicate the presence of elements such as titanium (Ti), calcium (Ca), magnesium (Mg), sodium (Na), zinc (Zn), silicon (Si), sulfur (S), chlorine (Cl), and potassium (K). This type of analysis is commonly used to determine the chemical composition of compound (ZnO:TiO_2) after.

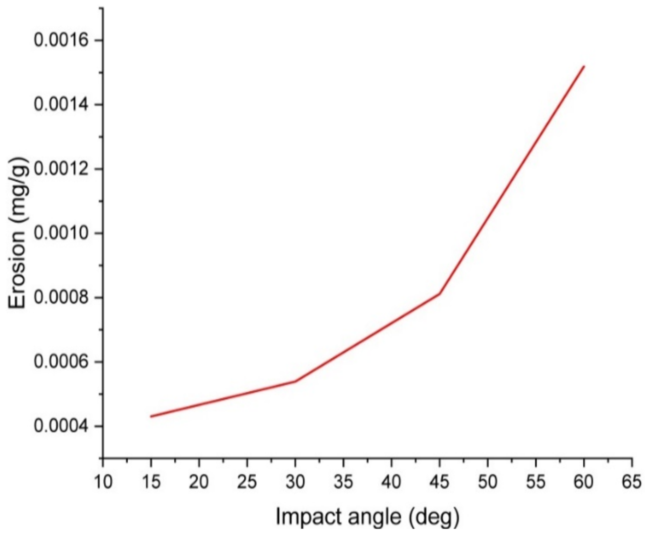

Fig. 10: Erosion of the ZnO 50%-TiO_2 50% nanocomposite with the impact angle of the sand particles.

Fig (10) illustrates how the sand particle impact angle affects the 50%-50% ZnO-TiO_2 coating's degradation rate. The erosion rate rises steadily as the impact angle increases, from roughly 0.0004 mg/g at 15° to roughly 0.0016 mg/g at 60°. The gradual increase between 15° and 45° indicates that as the normal component of the impact force increases, the coating undergoes incremental surface degradation. Improved material erosion at greater impact angles is indicated by a more noticeable increase between 45° and 60°. This behavior is typical of brittle materials, where crack initiation and propagation rather than cutting or plowing mechanisms are the main factors controlling erosion. Higher impact angles cause the usual impact stress to take over, which encourages the development of lateral and radial cracks beneath the coating surface. Increased erosion loss and coating fragment spallation are the results of these cracks spreading and coalescing. The greatest erosion rate observed at 60° suggests that the degradation of the 50%-50% ZnO-TiO_2 covering during sand-particle bombardment is mostly caused by normal impact pressures. This pattern implies that brittle fracture processes govern the erosion mechanism, resulting in increasing material removal and progressive surface deterioration as the impact angle gets closer to normal incidence [14].

4. Conclusion

This study successfully evaluated 50%-50% ZnO-TiO_2 nanocomposite coatings as a thin film for solar modules against desert-induced erosion. Structural characterization via XRD, SEM, EDX, and AFM confirmed a high-purity crystalline matrix with crystallite sizes **of** 31–33 nm**.** Critically, Erosion testing revealed a significant mass loss increase from ~0.0004 mg/g at 15° to ~0.0016 mg/g at 60°, identifying brittle fracture mechanics driven by crack propagation and spallation as the primary degradation mode. Despite surface particle fragmentation, the coating's strong adhesive force prevented its complete removal from the glass substrate. Ultimately, this work provides an essential reference for enhancing the maintenance schedules and operational efficiency of solar plants in harsh, sand-intensive environments. By mastering the mechanical durability of these multifunctional films, We strive to overcome the challenges posed by sandy environments to ensure the success of the global transition toward energy sustainability.

References

[1] S. Guo, Y. Cui, Z. Zhang, L. Cao, T. Wu, and B. Li, "Synthesis of ZnO-TiO2-Amygdalin NCs and its bio application," *Scientific Reports*, June 2025.

[2] A. Patnaik, S. Biswas, R. Kaundal, and A. Satapathy, "Damage Assessment of Short Glass Fiber Reinforced Polyester Composites: A Comparative Study," in *Nanocomposites with Unique Properties and Applications in Medicine and Industry*, J. Cuppoletti, Ed. Rijeka, Croatia: InTech, 2011, pp. 125-132.

[3] C. Cheng, A. Amini, C. Zhu, Z. Xu, H. Song, and N. Wang, "Enhanced photocatalytic performance of TiO2-ZnO hybrid nanostructures," *Scientific Reports*, vol. 4, p. 4181, 2014.

[4] E. H. M. Fares, "Enhancing the Performance of Photovoltaic (PV) Panels Using Anti-Soiling Coatings Techniques," Ph.D. dissertation, Hamad Bin Khalifa University, Doha, Qatar, March 2022.

[5] X. Liu, N. Wang, M. Zhao, and X. Hu, "Experimental Study on the Effect of Sand and Dust on the Performance of Photovoltaic Modules in Desert Areas," *Energies*, vol. 17, no. 3, p. 682, 2024.

[6] Z. Zhang et al., "Experimental investigation of a monitoring model for dust deposition on solar photovoltaic," *International Journal of Green Energy*, 2023.

[7] V. Bonu and H. C. Barshilia, "High-Temperature Solid Particle Erosion of Aerospace Components: Its Mitigation Using Advanced Nanostructured Coating Technologies," *Coatings*, vol. 12, no. 12, p. 1979, 2022.

[8] A. K. Padhan, V. Singh, S. Ray, and R. K. Voolapalli, "High-performance multi-functional solar panel coatings: recent advances, challenges, strategies and industrial aspects," *RSC Applied Polymers*, vol. 3, p. 317, 2025.

[9] H. McI. Clark and K. K. Wong, "Impact angle, particle energy and mass loss in erosion by dilute slurries," *Wear*, vol. 186-187, pp. 454-462, 1995.

[10] Y. I. Oka, S. Mihara, and T. Yoshida, "Impact-angle dependence and estimation of erosion damage to ceramic materials caused by solid particle impact," *Wear*, vol. 267, pp. 129–135, 2009.

[11] X. Liu et al., "Mechanism underlying the effect of physical properties on the dynamic behaviours and erosion characteristics of particles on solar photovoltaic panels," Wuhan University of Science and Technology, 2020.

[12] M. L. Adekanbi, E. S. Alaba, T. J. John, T. D. Tundealao, and T. I. Banji, "Soiling loss in solar systems: A review of its effect on solar energy efficiency and mitigation techniques," *Cleaner Energy Systems*, vol. 7, p. 100094, 2024.

[13] I. El-Mahallawi et al., "Solar PV Panels-Self-Cleaning Coating Material for Egyptian Climatic Conditions," *Sustainability*, vol. 14, no. 17, p. 11001, 2022.

[14] J. Alqallaf, N. Ali, J. A. Teixeira, and A. Addali, "Solid Particle Erosion Behaviour and Protective Coatings for Gas Turbine Compressor Blades—A Review," *Processes*, vol. 8, no. 8, p. 984, 2020.

[15] M. Kaplan, M. Uyaner, E. Avcu, Y. Y. Avcu, and A. C. Karaoglanli, "Solid particle erosion behavior of thermal barrier coatings produced by atmospheric plasma spray technique," *Mechanics of Advanced Materials and Structures*, vol. 25, no. 14, pp. 1-7, 2018.

[16] B. Zhang, J. Wang, Z. Shi, Q. Liu, and G. Ji, "Study on Sand Erosion and Tribological Behavior of TiO2 Films Prepared on a Glass Surface," *Journal of Nanoscience and Nanotechnology*, vol. 18, no. 3, pp. 1792–1798, 2018.

[17] C. O. Rusănescu, M. Rusănescu, I. A. Istrate, G. A. Constantin, and M. Begea, "The Effect of Dust Deposition on the Performance of Photovoltaic Panels," *Energies*, vol. 16, no. 19, p. 6794, 2023.

[18] A. Franco and S. G. Roberts, "The effect of impact angle on the erosion rate of polycrystalline α-Al2O3," *Journal of the European Ceramics Society*, vol. 16, pp. 1365-1375, 1996.

[19] Y. Zhao, R. Liu, F. Yan, D. Zhang, and J. Liu, "Windblown Sand-Induced Degradation of Glass Panels in Curtain Walls," *Materials*, vol. 14, no. 3, p. 607, 2021.

[20] X. Liu, N. Wang, M. Zhao, and X. Hu, "Experimental Study on the Effect of Sand and Dust on the Performance of Photovoltaic Modules in Desert Areas" (Second Entry), *Energies*, vol. 17, p. 682, 2024.

[21] Encyclopedia.pub, "Erosive Wear Characteristics of Cermets and Ceramic-Metal Composites," Review retrieved from encyclopedia.pub.

[22] Sahar Abdul Aziz , Reem Sami Ali , Ahmed N. Abd , Characterization studies of nickel oxide nanostructure films prepared by electrolysis method for photo detectors applications, NeuroQuantology ,18(2):45-49 ,DOI: 10.14704/nq.2020.18.2.NQ20123

[23] Ahmed N. Abd , Mohammed F. Al –Marjani and Zahraa A. Kadham , Synthesis of CdO NPS for antimicrobial activity, Int. J. Thin. Fil. Sci. Tec. 7, No. 1, 43-47 (2018), doi:10.18576/ijtfst/070106

[24] Hassoni, Majid H. ; Aziz, Wisam J.; Abd, Ahmed N.; Habubi, Nadir F. Invention and description of p-CuO/n-Si (200°C) heterojunction for photodiode applications,11(2)2019

[25] Shakeel, N.; Piwoński, I.; Iqbal, P.; Kisielewska, A. Green Synthesis of titanium dioxide nanoparticles: Physicochemical characterization and applications: A review. Int. J. Mol. Sci. 2025, 26, 5454. [Google Scholar]

[26] Thakur, B.K.; Kumar, A.; Kumar, D. Green synthesis of titanium dioxide nanoparticles using azadirachta indica leaf extract and evaluation of their antibacterial activity. S. Afr. J. Bot. 2019, 124, 223–227.